ULTRA SMALL-ANGLE X-RAY SCATTERING STUDY OF FLOCCULATION IN SILICA-FILLED RUBBER

Satoshi Mihara,[1] Rabin N. Datta,[2] Wilma K. Dierkes,[2] Jacques W.M. Noordermeer,[2*] Naoya Amino,[1] Yasuhiro Ishikawa,[1] Shoutaro Nishitsuji,[3] and Mikihiko Takenaka[3]

[1] The Yokohama Rubber Company, Ltd., 2-1 Oiwake, Hiratsuka, Kanagawa, 254-8601, Japan

[2] Department of Elastomer Technology and Engineering, Faculty of Engineering Technology, University of Twente, P.O. Box 217, 7500 AE Enschede, the Netherlands

[3] Department of Polymer Chemistry, Graduate School of Engineering, Kyoto University, Katsura, Nishikyo-ku, Kyoto 661-8510, Japan

* Corresponding author: E-mail: j.w.m.noordermeer@utwente.nl, tel: +31 53 489 2529, Fax: +31 53 489 2151

ABSTRACT

In this study the flocculation of silica during vulcanization is monitored using the USAXS technique for two different types of silica: a highly dispersible silica (HD) and a conventional silica (CV), mixed into a blend of S-SBR and BR rubbers. The cutoff length of the silica aggregate R_{ss} and the mass fractal dimension D_m, which indicate the degree of flocculation of aggregates, are estimated according to the modified unified equation. The aggregate radius R_a is estimated to be related to the lower cut-off length R_{ss}, indicating the radius of gyration of the mass-fractal structure. For both silicas R_a increases during vulcanization. For the CV silica an increase of D_m is observed, whereas no significant increase of D_m can be seen for the HD silica. R_a of CV is a relatively high compared to that of HD. On the other hand, the CV silica shows a relatively lower D_m compared to that of HD. These results indicate that CV has a larger size of aggregates and lower degree of agglomeration of its aggregates. The presence of TESPT as coupling agent between the silica and rubber decreases the aggregate radius of silica. However, in the absence of TESPT a low mass-fractal dimension, which means a low degree of agglomeration of aggregates, is observed. This results from a lower mobility of silica aggregates, depending on the size of the aggregates. The silica loading also has an influence on the flocculation process. The aggregate radius increases as the silica loading is increased. At the same time, a higher mass-fractal dimension, therefore also higher degree of agglomeration can be seen at higher silica loading.

Introduction

Filler dispersion in rubber compounds plays an important role in the physical properties of reinforced rubber. The dispersion of filler in a rubber matrix strongly depends on the polarity difference between polymer and filler, such as carbon black or silica.

It is generally known that the hierarchical structure of fillers such as the primary particles, aggregates and agglomerates can still be recognized in a filled rubber. The presence of remaining agglomerates strongly negatively affects the reinforcing properties of the fillers in rubber, while the aggregates are the real reinforcing species. The reinforcing properties strongly depend on the following factors: (1) the degree of physically linked aggregates in the filler network, as often quantified by the Payne effect, and (2) polymer-filler interaction, for example described as bound rubber.

The relationship between the morphological properties of silica and the reinforced properties of rubber is not fully understood. Many morphological studies such as with TEM microscopy and measurement of the electrical percolation threshold have been done in the past to investigate the filler structure [1-8]. For 3-dimensional observations using TEM, a high volume fraction of fillers such as commonly used in typical tire tread compounds, leads to difficulties discern the filler structure, because of an overlap of the structure along the electron beam direction. In addition, the special thin sample of 50-100nm thickness required for a TEM observation, smaller than the average aggregate size of the filler, also lead to difficulties with respect to a 3-dimensional observation. Measurement of the electrical percolation threshold is a useful technique for a carbon black filled compound because of its high conductivity. However, this measurement can not be applied to silica filled-compounds due to lack of conductivity.

For 3-dimensional characterization of filler-filled compounds, small angle scattering is a useful technique to understand the morphological properties of fillers in a rubber matrix. Ultra small angle scattering (USAS) and small angle scattering (SAS) using X-rays, neutrons and visible light have been widely used earlier to investigate the morphological structure of fillers in rubber matrices [9-13].

In the present study, ultra small angle X-ray scattering (USAXS) which can cover a scattering angle q range of 0.01 to 0.4nm^{-1} is applied to characterize the filler morphology in a rubber compound. The focus is on silica-flocculation in a rubber compound during vulcanization. It is worthwhile to mention in this context that the activation energy of silica flocculation was quantified earlier to be approximately 10 kJ/mole, indicating that silica flocculation is a purely physical phenomenon [14]. In addition, Reuvekamp et al. proposed that the flocculation of the silica takes place at the very beginning of the vulcanization [15].

This paper focusses on the morphological properties of the silica during vulcanization. The structural-hierarchical parameters such as the mass-fractal dimension and the size of the aggregates are estimated using the Beaucage unified equation, which is composed of a Guinier scattering function combined with a power-law scattering. Based on the differences of the structural parameters between highly dispersible silica and conventional silica, the morphological property changes in the rubber compound will be investigated during the temperature treatment involved in vulcanization.

Experimental

Sample preparation.- The compound formulations are based on a typical tire tread compound according to the fuel-saving green tire technology as shown in Table 1. In the present study two types of silica, a highly dispersible silica and a conventional silica are used. Structural analytical data of the silicas are shown in Table 2. The amount of Bis(tri-Ethoxy-Silyl-Propyl)Tetrasulfide (TESPT) coupling agent between the silica and rubber in the recipes was adjusted according to equation 1, which is related to the CTAB (Cetyl Tri-Ammonium Bromide) surface area of the silicas [16]:

$$TESPT\ (phr) = 5.3 \times 10^{-4} \times (CTAB)_{silica} \times (phr)_{silica} \qquad (1)$$

The total amount of active sulfur was adjusted to 2.1 phr, being the sum of the sulfur contained in the

silane and in the curatives.

The compounds were mixed in 3 steps. The first two steps were done using a tangential type internal mixer with 1.7L volume. The mixing procedures are shown in Table 3. The starting temperature of the mixing chamber was 60˚C. The dump temperature in the first two steps was kept below 160˚C by changing the rotor speed. The fill factor of the mixer was fixed to 65%. The curatives were mixed on the two roll mill in the third step.

Ultra small-angle X-ray scattering (USAX) measurement.- The USAXS measurement was done at ambient pressure by using the Spring-8 (Super Photon ring-8, Beam line BL19B2, Japan Atomic Energy Research Institute); world's largest third-generation synchrotron radiation facility. The time division method was applied in the present investigation. A layout of the measurement system is described in Figure 1. The X-ray scattering was detected using the pixel detector (PILTUS) covering the q-range of 0.01～0.4 nm^{-1} ($q=(4\pi/\lambda)\sin\theta$: θ=scattering angle ; λ=wave length of the X-ray=0.5 Å [24 keV]). The distance between the sample and the PILTUS is approximately 40 m, therefore the ultra small-angle scattering X-rays can be detected.

The silica filled rubbers of about 1 mm thickness were held in the thermostatic chamber at the specified temperature for 1500 sec. Data correction was done for sample transmission and for background scattering arising from air and fused quartz in the thermostatic chamber.

Data analysis.- A schematic scattering profile combining ultra small-angle neutron scattering (USANS), ultra small-angle X-ray scattering (USAXS) and small angle X-ray scattering (SAXS) for a precipitated silica are shown in Figure 2 [11, 12]. At least three separate levels of the structure of silica can be detected, corresponding to morpholog00ical properties such as the size of the primary particles, the degree of aggregation or agglomeration and the surface profile of the particles.

In general, for the scattering data as shown in Figure 2, a curve fitting using a unified approach

developed by Beacauge is applied for estimation of the structural parameters such as R_{ss} and R_{gg} corresponding to the size of aggregates and agglomerates, respectively. The power-law scattering profile is described as in equation 2 [17].

$$I(q) \cong q^{-p} \qquad (2)$$

where I(q) is the scattering intensity at the scattering angle q and p is the power law exponent.

In the high q region the scattering intensity decays following Porod's law. The power law value p=4 indicates the scattering from the smooth surface of the particles. However, it is well known that the filler surface such as of carbon black and silica is not smooth but rough [18, 19]. In this case, the surface fractal dimension (D_s) is related to the power-law exponent p as follows:

$$p = 2d - D_s \qquad (3)$$

where d is the Euclidean dimension of the space (d=3) and D_s is the surface fractal dimension. If I(q) is plotted as a function of q logarithmically, the slope of ln (I(q)) vs. ln (q) plot can vary between -3 and -4. On the other side, at low q, the so-called Guinier region, the scattering intensity decays following Guinier's law. The decay of the scattering intensity in this region can be described as shown in equation 4:

$$I(q) \cong I(0)\exp\left(-\frac{q^2 R_i^2}{3}\right) \qquad (4)$$

where R_i is the structural size of aggregates or agglomerates.

At low scattering angles q two Guinier regions, which mean the two levels of aggregate and agglomerate sizes, can be seen. As shown in Figure 2, two discrete shape-factor profiles such as R_{gg}^{-1} and R_{ss}^{-1} can be seen, which can be derived from the Guinier scattering function equation 4. R_{gg}^{-1} and R_{ss}^{-1} indicate the upper and lower cut-off length of the mass-fractal structure, respectively. The power-law scattering between these two Guinier regions indicates the mass-fractal structure D_m. In fact, the power-law slope in this region means the mass-fractal dimension, therefore the power law index p in equation 5, is characterized as follows [13]:

$$p = D_m \qquad (5)$$

For the qualitative analysis of the structural parameters based on the unified equation, the following equation is applied to the scattering profiles in the present study [13].

$$I(q) = A\exp\left(-\frac{q^2R_{gg}^2}{3}\right)q^{-p} + B\exp\left(-\frac{q^2R_{gg}^2}{3}\right) + C\exp\left(-\frac{q^2R_{ss}^2}{3}\right)\times\left[\mathrm{erf}\left(\frac{qR_{gg}}{\sqrt{6}}\right)\right]^{3D_m} q^{-D_m} + D\exp\left(-\frac{q^2R_{ss}^2}{3}\right) + E\left[\mathrm{erf}\left(\frac{qR_{ss}}{\sqrt{6}}\right)\right]^{3(2d-D_s)} q^{-(2d-D_s)} \qquad (6)$$

where R_{gg} and R_{ss} are the upper (agglomerates) and lower (aggregate) cut-off length of the mass-fractal structure, respectively, and A, B, C, D and E are constants.

In the present study, no upper cut-off length (R_{gg}) for the mass-fractal structure can be seen in the covered q, as will be described later. Therefore, R_{gg} is assumed as an infinite value. As a result, the first two terms in equation 6 can be neglected and the third term, which is an error function, can be taken constant. Taking these assumptions into account, equation 6 can be simplified as follows [13]:

$$I(q) = C\exp\left(-\frac{q^2R_{ss}^2}{3}\right)\times q^{-D_m} + D\exp\left(-\frac{q^2R_{ss}^2}{3}\right) + E\left[\mathrm{erf}\left(\frac{qR_{ss}}{\sqrt{6}}\right)\right]^{3(2d-D_s)} q^{-(2d-D_s)} \qquad (7)$$

By using equation 7, the structural parameters such as R_{ss} and D_m are estimated in the present study. The lower cut-off length R_{ss} indicates the radius of gyration of the mass-fractal structure.

Results

Comparison of the structural parameter between highly dispersible and conventional silica.- Figures 3 (a) and (b) show examples of USAXS scattering profiles for the highly dispersible silica and the conventional silica at different times. For both silicas, one form-factor profile (R_{ss}^{-1}), as assumed by a

Guinier scattering profile, is observed. In addition, two different slopes at high and low q are visible, which indicate mass-fractal structures with mass-fractal dimension (D_m) and the primary particles with their surface fractal dimension. The power-law values p at high q do not show a value of p=4, but 3.3 and 3.1, respectively. This means that the surface of the primary particles is not smooth.

In order to investigate the silica flocculation phenomenon, the radius of gyration cut-off length R_{ss} and the mass-fractal dimension D_m for each silica were estimated according to equation 7. Based on the assumption that the shape of aggregates is spherical with radius R_a, the radius of gyration R_{ss} can be described in relation to R_a as follows [11, 13, 17]:

$$R_{ss} = \sqrt{\frac{3}{5}} \times R_a \qquad (8)$$

In the present study we therefore can assume that R_{ss} and D_m indicate the size of aggregates and the degree of the agglomeration of the aggregates, respectively.

Figures 4 (a) and (b) show the estimated radius of the silica aggregates as a function of vulcanization time at the different temperatures. The aggregate radius of the CV silica is relatively high compared to that of the HD silica. In addition, the aggregate radius of the CV silica increases slightly faster than that of HD silica as temperature and time are raised. This translates in the fact that the flocculation rate of the CV silica is relatively fast compared to that of the HD silica. This tendency of increasing aggregate size corresponds to the flocculation rate estimated by the RPA2000 measurements [14]. Indeed, the aggregate radius of the HD silica and the CV silica can be estimated as 24 to 26 nm and 33 to 37 nm, respectively. At the highest vulcanization temperature of 160˚C, the aggregate radius increases quickly till a vulcanization time of 10 minutes and then remains unchanged. This means that once the crosslinking reaction proceeds, silica flocculation does not take place any more.

Figures 5 (a) and (b) show the mass-fractal dimension D_m as a function of the vulcanization time at the different temperatures. For both silicas D_m increases with an increase of vulcanization temperature. However, in the case of the HD silica, no significant change of D_m during vulcanization can be seen except for the vulcanization temperature of 160˚C. For the CV silica it is clearly seen that D_m increases

with increasing vulcanization time. It is interesting to find that the mass-fractal dimension of the CV silica is relatively low compared to that of the HD silica, while the R_{ss} of the CV silica is higher than that of the HD silica.

Effect of the filler loading on the structural parameters.- Figures 6(a) and (b) show the radius of aggregates with different silica loading as a function of vulcanization time. As is evident from Figures 6(a) and (b) for both silicas, a higher R_a is found especially for higher silica loading.

Figures 7 (a) and (b) show the mass-fractal dimension with different silica loading as a function of vulcanization time. For both silicas, D_m increases as the vulcanization proceeds. In addition, with increasing silica loading, D_m increases. Again, D_m of the CV silica is relatively low compared to that of the HD silica.

Effect of the presence of silane on the structural parameters.- The effect of the presence of TESPT on the structural parameters was investigated and the results are shown in Figures 8 (a) and (b). In the absence of TESPT, the aggregate radius R_a of the HD silica increases. The higher R_a can be related to a lower mobility of the aggregates as will be discussed later. In addition, the mass-fractal dimension D_m is relatively low in the absence of TESPT, which means a lower degree of the agglomeration of the aggregates.

Discussion

It was observed that the lower cut-off length R_{ss}, which indicates the radius of gyration of the silica aggregate, increases during vulcanization. In addition, an increase of D_m the mass-fractal dimension, was seen. It is known that the spherical aggregate of radius R_a is linked to R_{ss}, hence the aggregates size increases during the vulcanization. From a morphological point of view, it can be mentioned that the

HD silica and the CV silica both have a primary particle diameter of approximately 14 nm. Therefore, the following mechanism regarding the hierarchical structure can be proposed as shown in Figure 9. It was found that the aggregate radius R_a of the HD silica and the CV silica were approximately 24-26 nm and 33-37 nm, respectively.

For the CV silica, the increase of aggregate radius R_a during vulcanization is relatively fast compared to the HD silica: Figure 4. This corresponds to the flocculation rate of the silicas estimated by previous vulcanization speed measurements [14]. In these measurements, an increase of storage modulus G' during a heating process was observed due to silica flocculation. This increase of G' could be related to an increase of the aggregate size. In fact, the present results conclusively indicate that the increase of the aggregate size results in the increase of the storage modulus in silica-filled rubber.

A next point to focus on is the degree of agglomeration of the aggregates. In the previous work, due to the fact that the activation energy of the silica flocculation is approximately 10 kJ/mol, it was indicated that silica flocculation is a purely physical phenomenon [14]. As stated before, for the estimation of the structural parameters such as the aggregate radius R_a and the mass-fractal dimension D_m, it was assumed that the shape of the aggregates or the agglomerates is spherical. Therefore, the mobility of the particles in terms of their diffusion constant D can be described by equation 9, the Stokes-Einstein equation [19]:

$$D = \frac{kT}{6\pi\eta r} \qquad (9)$$

where: D is the diffusion coefficient, k is Boltzmann's constant, T is the absolute temperature, η is the viscosity of the matrix and r is the hydrodynamic radius of the particle.

The aggregate radius of the CV silica is relatively high compared to that of the HD silica. This indicates that the hydrodynamic radius r of the CV silica is relatively high in comparison with the HD silica. As a result, the mobility of aggregates of the CV silica can be low according to equation 9. This low mobility of the aggregates then leads to a lower degree of agglomeration of aggregates D_m.

The silica loading also influences the morphological properties of filled rubber. In Figure 6, the radius of aggregates is higher as the silica loading is increased. The degree of agglomeration of the aggregates

D_m also increases with higher silica loading. The attractive force between the particles depends on their mutual distance. In other words, the correlation length between the particles, which means that the particles can attract each other, increases with higher silica loading. As a result, the degree of flocculation of aggregates increases, which is observed as an increase of the mass-fractal dimension D_m. Therefore, the degree of silica loading is one of the dominant factors for the flocculation process in silica-filled rubber.

In view of the previous results, the effect of the coupling agent TESPT can now also easily be understood. The polarity difference between silica and the polymers play an important role in the morphology of the rubber matrix. TESPT reduces the polarity difference between silica and polymer. In the absence of TESPT, the aggregate radius R_a is obviously larger as shown in Figure 8, due to a higher driving force for demixing. On the other hand, the degree of the agglomeration of aggregates D_m then decreases, due to a decrease of mobility of the aggregates.

Conclusions

The USAXS technique is useful for real time analysis of silica flocculation. The aggregate size of the CV silica is relatively high compared to that of the HD silica. The aggregate radii R_a for the HD silica and the CV silica can be estimated as 24-26nm and 33-37 nm, respectively.

The aggregate radius of the CV silica increases fast during vulcanization compared to the HD silica. This result corresponds with the flocculation rate of silica, as estimated by from vulcanization speed measurements [14]. On the other hand, for the CV silica, the degree of agglomeration of the aggregates D_m is relatively lower than for the HD silica. This results from the lower mobility of the aggregates because of large aggregate size.

An increase of silica loading causes the aggregate radius R_a and the mass-fractal dimension of the

agglomerates D_m to increase as well. TESPT plays an important role in the reducing the aggregate radius R_a of silica. In the absence of TESPT an increase in aggregates radius was found. Since the mass-fractal dimension D_m strongly depends on the aggregate size of silica, corresponding to physical diffusion of filler aggregates, in the absence of TESPT a lower mass fractal dimension, which means a decrease of the mobility of the aggregates, was observed.

The present results again confirm that silica flocculation is a physical phenomenon, as already demonstrated in our previous work [14].

Acknowledgement

This project was financially supported by the Yokohama Rubber Company LTD.

References

1. Medalia, AJ. J. Colloid Interface Sci., 1967, 24, 393
2. Hess, WM; Ban, LL; McDonald, GC. Rubber Chem. Tech., 1969, 42, 1209
3. Hess, WM; McDonald, GC; Urban, EM. Rubber Chem. Tech., 1972, 44, 204
4. Herd, CR; McDonald, GC; Hess, WM. Rubber Chem. Tech., 1992, 65, 107
5. Medalia, AJ. Rubber Chem. Tech., 1986, 59, 432
6. Ouyang, GB. Kautsch. Gummi Kunstst., 2002, 55, 104
7. Gefen, Y; Aharony, A; Alexander, S. Phys. Rev. Lett., 1983, 50, 77
8. Stroud, D; Bergman, DJ. Phys. Rev. B, 1982, 25, 2061
9. Klüppel, M; Heinrich, G. Rubber Chem. Techn., 1995, 68, 623
10. Göritz, D; Schneider, GJ. Kautschuk HerbstKolloquium DIK, Hannover, Germany 10-13 Nov. 2004
11. Kohls, DJ; Schaefer, DW. Paper No. 68 presented at the Fall 170th Technical Meeting of the Rubber Division, Am. Chem. Soc., Cincinnati, OH, 10-12 Oct. 2006
12. Schaefer, DW; Kohls, DJ. Paper No. 69 presented at the Fall 170th Technical Meeting of the Rubber Division, Am. Chem. Soc., Cincinnati, OH, 10-12 Oct. 2006
13. Koga, T; Hashimoto, T; Takenaka, M; Aizawa, K; Amino, N; Nakamura, M, Yamaguchi, D; Koizumi, S.

Macromolecules, 2008, 41, 453

14. Mihara, S; Datta, RN; Dierkes, WK; Noordermeer, JWM. Paper No. 63 presented at the Fall 172th Technical Meeting of the Rubber Division, Am. Chem . Soc., Cleveland, OH, 16-18 Oct. 2007
15. Reuvekamp, LAEM; Debnath, SC; Ten. Brinke, JW; Van. Swaaij, PJ, Noordermeer, JWM. Rubber Chem. Techn., 2004, 76, 43
16. Wolff, S; Wang, MJ; Tan, EH. Rubber Chem. Techn., 1993, 66,163
17. Beaucage, GJ. J. Appl. Crystall., 1995, 28, 717
18. Rieker, TP; Hindermann-Bischoff, M. Langmuir,2000, 16, 5588
19. Schmidt, PW. J. Appl. Crystall.,1991, 24, 414
20. Böhm, GG; Nguyen, M. J. Appl. Polym. Sci. , 1995, 55, 1041

Table 1: Compound formulations.

Component	Product name	Supplier	phr
S-SBR[1]	Buna VSL5025	HM-1 Lanxess	103.1
BR	Nipol 1220	Nippon Zeon	25
Silica	listed in Table 2	listed in Table 2	80
Silane (TESPT)	Si69	Degussa	0 or as listed in Table 2
Aromatic oil	Tudalen 3570A	Hansen & Rosenthal	4.4
Zinc oxide	ZnO	Merck	2.5
Stearic acid		Merck	2.5
Sulfur		J.T. Baker	Variable
CBS[2]	Santocure CBS	Flexsys	1.7
DPG[3]	Perkacit DPG	Flexsys	2.0

[1] 37.5 phr oil-extended

[2] CBS: N-Cyclohexyl Benzothiazol Sulfenamide

[3] DPG: Di-Phenyl Guanidine

Table 2: Structural analytical data of the silica types.

Code	Product name	Source	BET[1] (m^2/g)	CTAB[2] (m^2/g)	DBP[3] (g/100g)	Silane loading (phr)
HD	Zeosil 1165MP	Rhodia Silices	155	152	196	6.4
CV	Ultrasil VN3	Degussa	177	168	183	7.1

[1] BET: Brunauer, Emmer and Teller specific surface area

[2] CTAB: Cetyl Trimethyl Ammonium Bromide specific surface area

[3] DBP: Di-Butyl Phtalate Adsorption Filler Structure

Table 3: Mixing procedures.

Step 1		**Step 2**		**Step 3**
Time	**Action**	**Time**	**Action**	**Action**
0.00	Add rubber	0.00	Add master batch	All curatives were mixed on a two-roll mill
1.00	Add ½ silica, ½ silane	1.00	Add ZnO	
2.00	Add ½ silica, ½ silane, oil, stearic acid	5.00	Dump	
4.00	Ram up, sweep			
4.20	Ram down			
6.20	Dump			

Captions to the figures:

Fig. 1: Schematic layout of USAXS equipment.

Fig. 2: Combined USANS, USAXS and SAXS profiles for silica powder.

Fig. 3: USAXS scattering profiles at 120 ^{o}C. (a): Highly dispersible silica 1165MP; (b): Conventional silica VN3. (o): 0 min; (Δ): 5 min; (□): 10 min; (◊): 15 min; (x): 20 min.

Fig. 4: Radius of aggregates R_a as a function of vulcanization time at specified temperatures. (a): Highly dispersible silica 1165MP; (b): Conventional silica VN3. (●): 90 ^{o}C; (o): 100 ^{o}C; (Δ): 120 ^{o}C; (x): 160 ^{o}C.

Fig. 5: Mass- fractal dimension D_m as a function of vulcanization time at specified temperatures. (a): Highly dispersible silica 1165MP; (b): Conventional silica VN3. (●): 90 ^{o}C; (o): 100 ^{o}C; (Δ): 120 ^{o}C; (x): 160 ^{o}C.

Fig. 6: Radius of aggregates R_a as a function of vulcanization time at different loadings of silica. (a): Highly dispersible silica 1165MP; (b): Conventional silica VN3. (●): 90 ^{o}C; (o): 100 ^{o}C; (Δ): 120 ^{o}C; (x): 160 ^{o}C.

Fig. 7: Mass-fractal dimension D_m as a function of vulcanization time at different loadings of silica. (a): Highly dispersible silica 1165MP; (b): Conventional silica VN3. (●): 60 phr; (o): 80 phr.

Fig. 8: Effect of TESPT on the structural parameters of silica 1165MP. (a): Radius of aggregates; (b): Mass-fractal dimension. (●): without TESPT; (o): with TESPT.

Fig. 9: Schematic model of morphological structure during vulcanization. (a): Highly dispersible silica 1165MP; (b): Conventional silica VN3.

Figure 1.

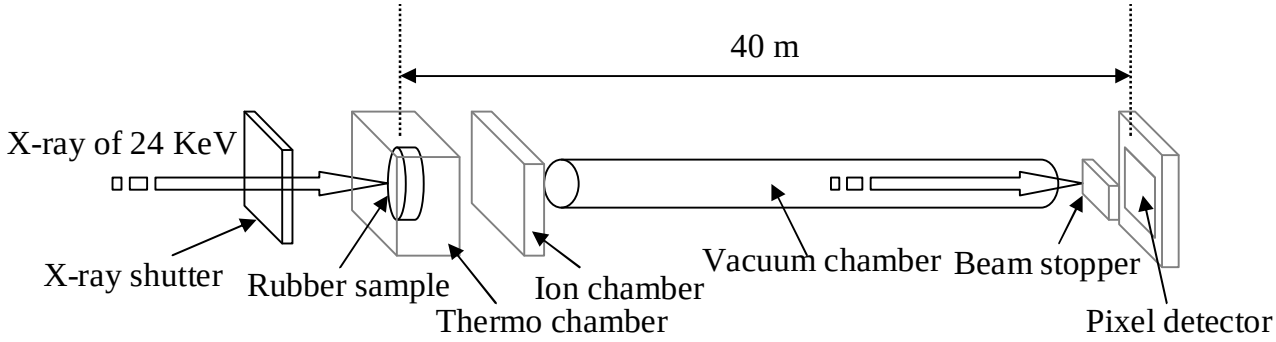
40 m
X-ray of 24 KeV
X-ray shutter
Rubber sample
Thermo chamber
Ion chamber
Vacuum chamber
Beam stopper
Pixel detector

Figure 2.

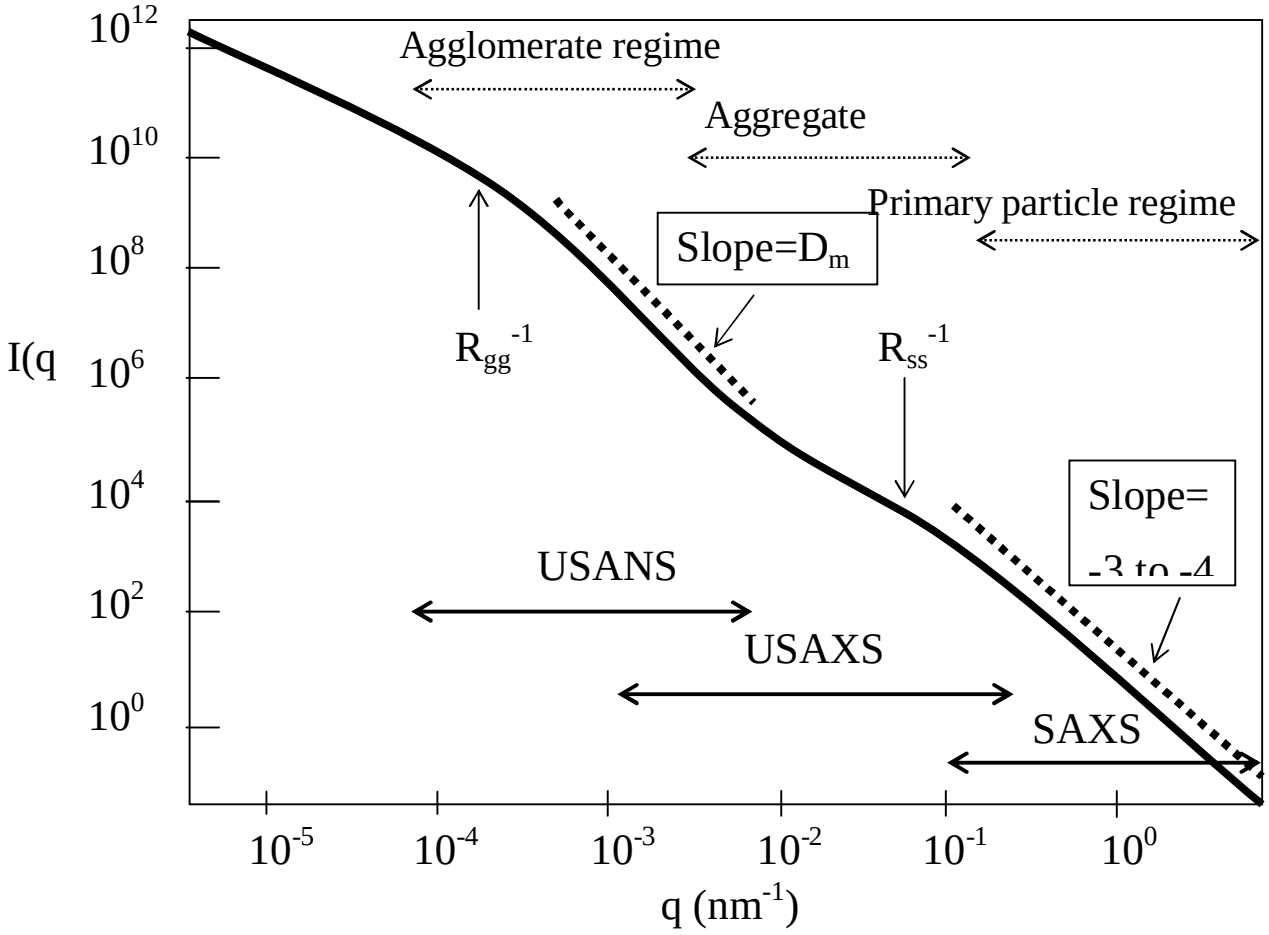
Agglomerate regime
Aggregate
Primary particle regime
Slope=D_m
R_gg^-1
R_ss^-1
Slope=
-3 to -4
USANS
USAXS
SAXS
I(q
10^12
10^10
10^8
10^6
10^4
10^2
10^0
10^-5
10^-4
10^-3
10^-2
10^-1
10^0
q (nm^-1)

Figure 3(a)

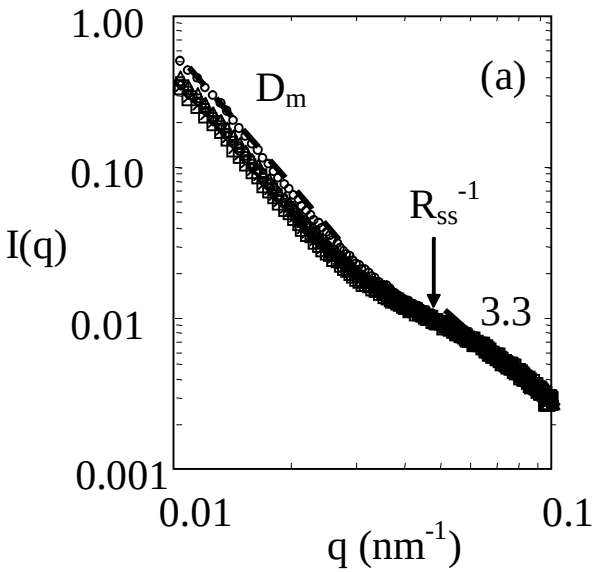

Figure 3(b).

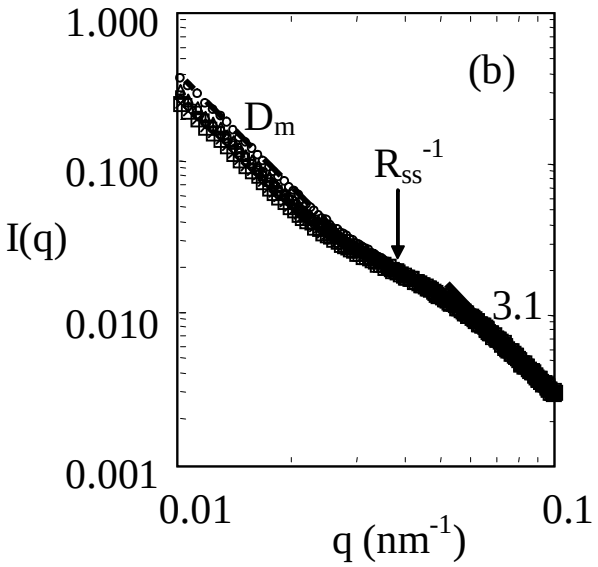

Figure 4 (a)

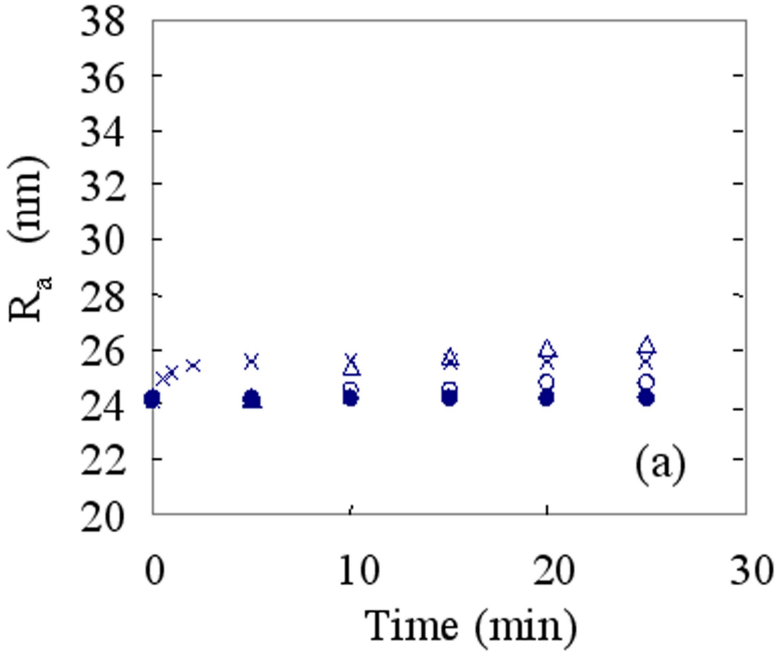

Figure 4(b)

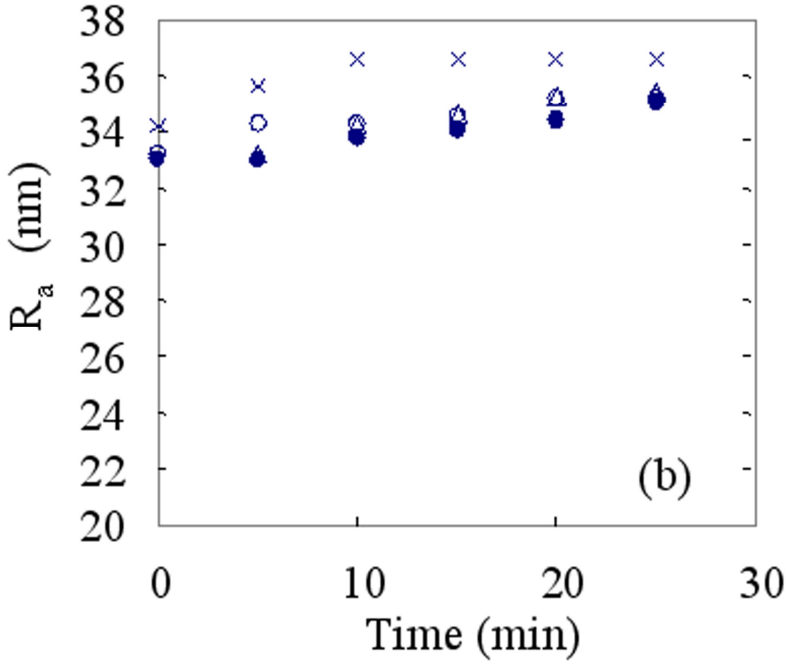

Figure 5 (a)

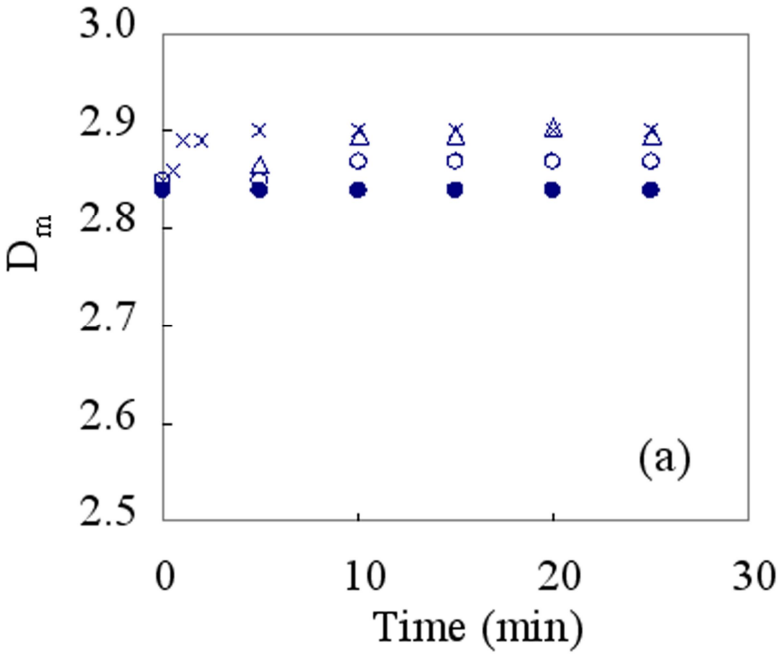

Figure 5 (b)

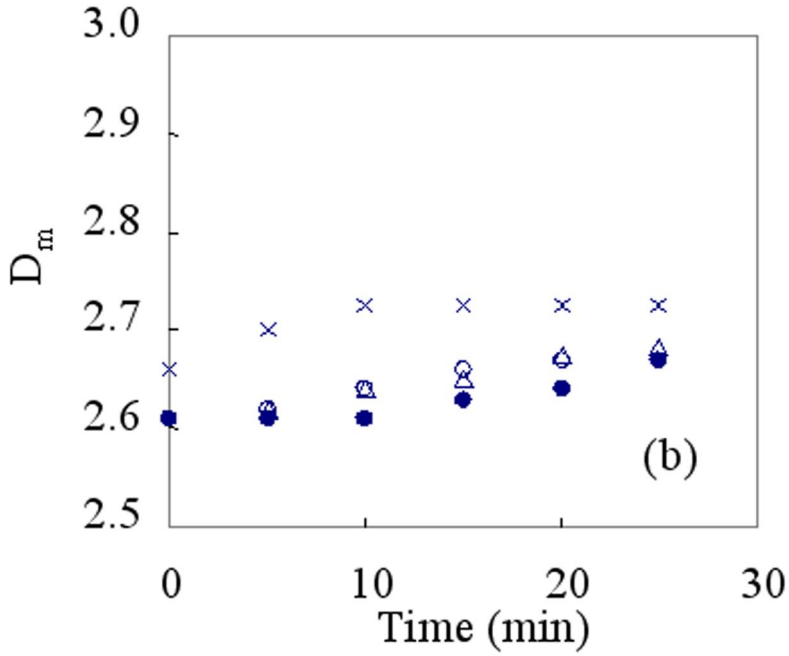

Figure 6 (a) .

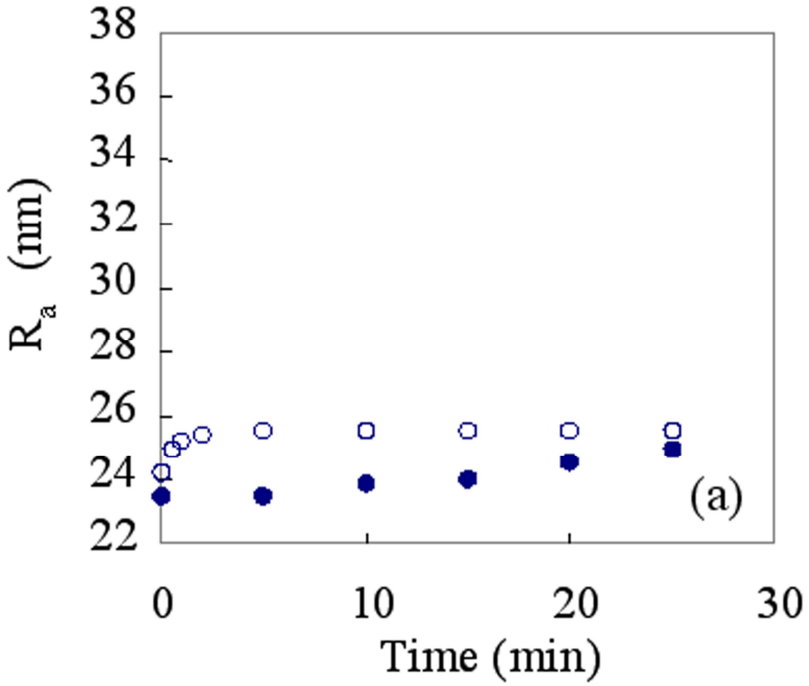

Figure 6 (b)

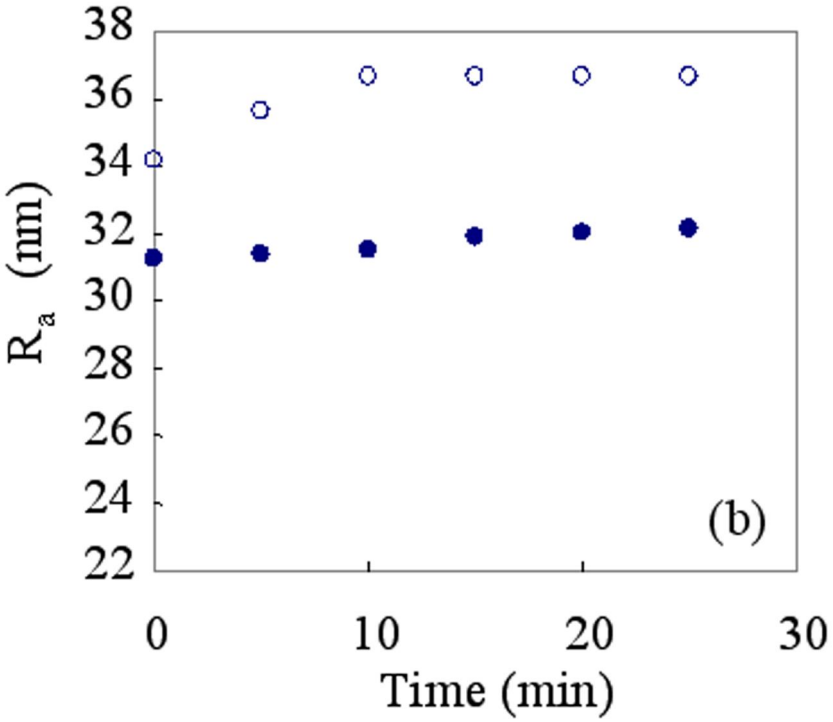

Figure 7 (a)

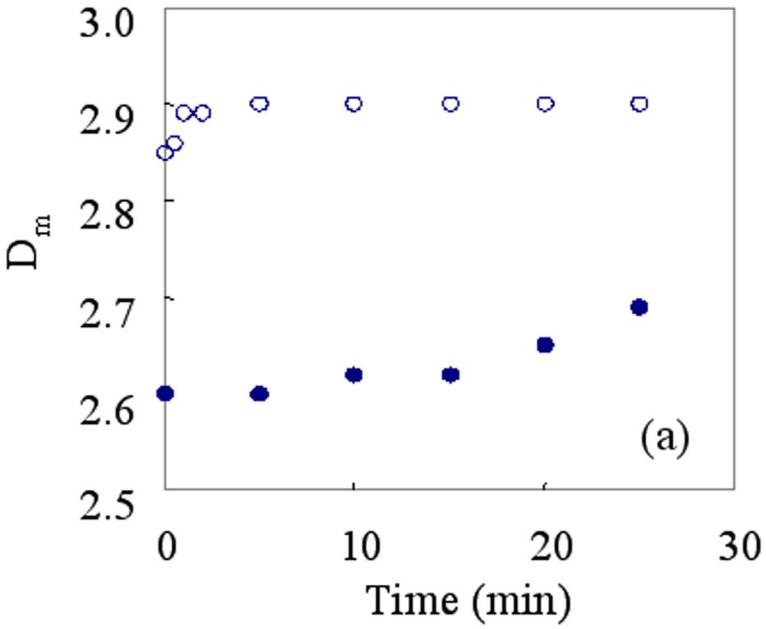

Figure 7 (b)

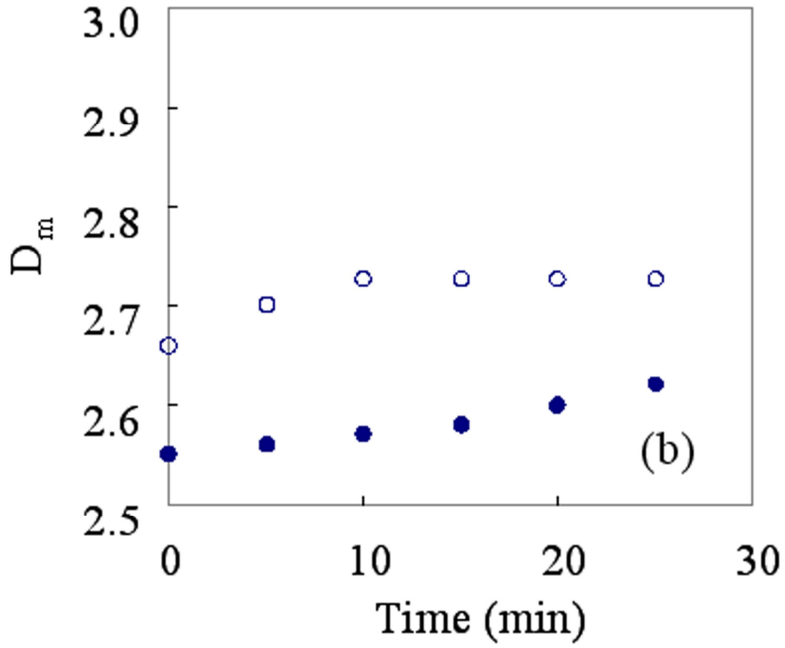

Figure 8 (a)

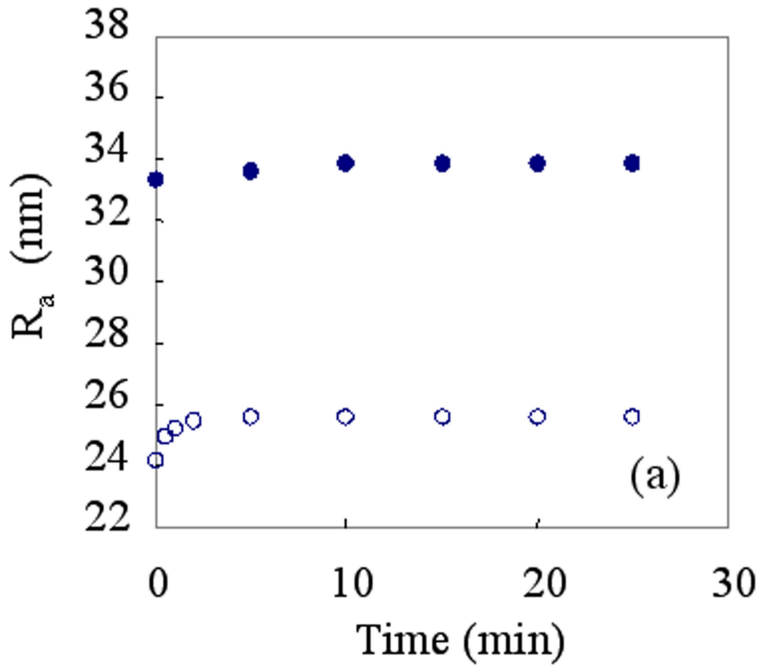

Figure 8 (b)

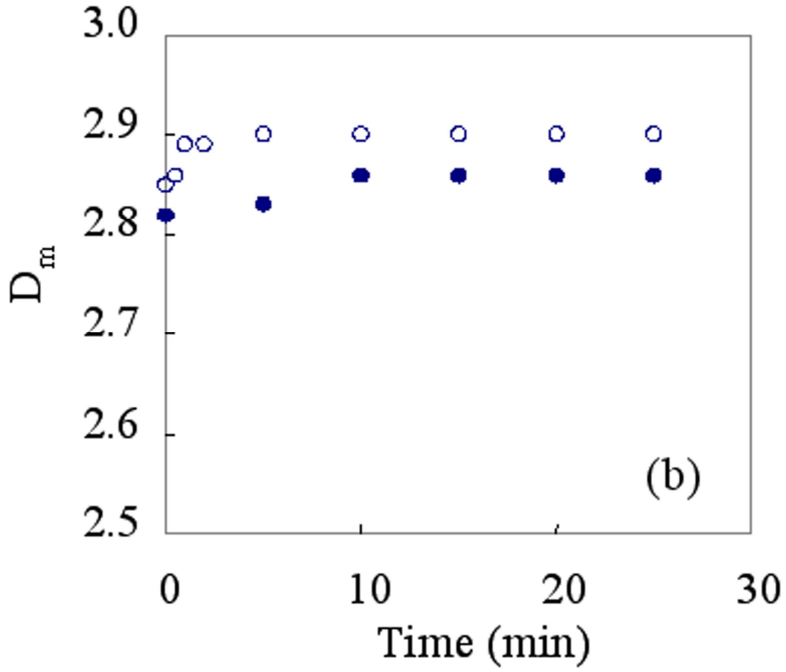

Figures 9 (a) and (b)